INTERNATIONAL JOURNAL FOR NUMERICAL AND ANALYTICAL METHODS IN GEOMECHANICS
Int. J. Numer. Anal. Meth. Geomech., **22**, 695–720 (1998)

UNI-AXIAL WAVE PROPAGATION AND PORE PRESSURE GENERATION IN FLUID SATURATED SANDS EXHIBITING IRREVERSIBLE COMPACTION

L. W. MORLAND[1] AND R. STAROSZCZYK[2]

[1] *School of Mathematics, University of East Anglia, Norwich NR4 7TJ, U.K.*
[2] *Institute of Hydroengineering, Polish Academy of Sciences, ul. Waryńskiego 17, 71-310 Szczecin, Poland*

SUMMARY

The propagation of a plane load–unload pulse through a compacting sand is analysed and illustrated for both dry sand and liquid saturated sand in undrained conditions. A major feature is the interaction between the initial loading wave and the faster following unloading wave. Free draining and undrained conditions exhibit distinct qualitative and quantitative results, and the pore liquid pressure generation is a significant physical feature. Illustrations show the effects of different applied surface pulse shapes.

Key words: wave propagation; compaction; pore pressure generation

1. INTRODUCTION

The dynamic response of both dry and liquid saturated granular materials is of particular importance in geomechanical areas. Shearing of loose or partly consolidated sands induces granular rearrangements which result in irreversible volume decrease—compaction—and irreversible shear strain, in addition to reversible elastic response. In dry sands the pores are filled with highly compressible air which supports little of the pressure, so even if the air is confined the sand behaves essentially like a free-draining (zero pore pressure) matrix. When the pores are filled with a liquid, water or oil for example, which has a low compressibility, then if there is confinement there can be a significant liquid pore pressure. For rapid disturbances caused by short time-scale surface loading, the drainage during a wave pulse or several sequential pulses will be negligible, inhibited by the interaction drag between the grains and liquid, and the response is then essentially that of an undrained matrix. Both free draining and undrained limits allow partial uncoupling of the laws governing the separate deformation of the sand and pore fluid, which leads to a single law for the total medium, and consequent simplification of the description of motion. Both limits are now exploited to analyse uni-axial wave propagation through dry and saturated sands, and explore pore pressure generation and pulse attenuation.

* Correspondence to L. W. Morland, School of Mathematics, University of East Anglia, Norwich NR4 7TJ, U.K.

CCC 0363–9061/090695–26$17.50

Received 20 November 1996
Revised 11 March 1997

Soil plasticity theories, reviewed by Zienkiewicz[1], to describe irreversible deformation are complex, and give rise to ill-posed boundary value problems, particularly for wave propagation. An alternative approach is the endochronic theory introduced by Valanis[2] in which evolution laws for the irreversible part of an infinitesimal strain are prescribed in terms of an accumulating deviatoric strain (scalar) measure, with no explicit dependence on time. This avoids the concepts of a yield surface and a flow rule. Bažant and Krizek[3,4] proposed such a differential law for the compaction of a saturated sand. A more systematic formulation for infinitesimal strain within the framework of a mixture theory for a porous solid[5,6] was presented by Morland and Sawicki[7,8] and then applied to cyclic shearing of dry and saturated sand columns by Sawicki and Morland[9,10]. Application of the basic model[7] to uni-axial displacement, and to a full treatment of shear strain involving necessary lateral stresses, revealed the inconsistency of ignoring the irreversible shear strain which accompanies granular re-arrangement, which prompted an extension of the theory to incorporate both irreversible compaction and irreversible shear strain[11], and the determination of restrictions necessary to avoid invalid initial shear response. A variety of model classes was explored to discover that only two could meet these requirements. The simpler one, using a total accumulated deviatoric strain measure as the monotonic loading parameter, was adopted by Morland *et al.*[12] to describe the uni-axial displacement response of a dry (free-draining) sand, and to correlate data from load–unload experiments. The response functions arising in the two simultaneous differential equations describing the uni-axial response were deduced for a particular sand and initial state, exhibiting good correlation except during the initial low stress loading. In turn, the differential relations predict the response to load–unload cycles to different maximum stresses. This occurs in a continuous manner as a loading wave is attenuated by a faster following unloading wave, which is the situation when a surface is subjected to a load–unload pulse.

This model for the dry sand is now extended to the undrained response when the pores are saturated by a liquid. While the dry sand model involved only the free-draining compressibility of the matrix, the undrained response involves also the undrained matrix compressibility and the intrinsic compressibilities of both liquid and sand grains. In addition, if the shear behaviour depends on effective pressure, total pressure less pore pressure, and not simply on total pressure, then in general there is coupling between relations for the matrix and the liquid. Since the undrained compressibility is far less than the free-draining compressibility, a good simplifying approximation is possible for the uni-axial stress–strain law for the matrix which is sufficient to determine an uncoupled matrix motion, and the pore pressure becomes a derived quantity. The propagation of plane load–unload pulses through both dry and undrained saturated sands is investigated with this basic model. The wave analysis is performed with a simplification of uniform (distinct) wave speeds for the separate loading and unloading responses, which allows straightforward treatment of the interaction between the loading and faster unloading wave at the separating moving interface. This is a crude approximation for the free-draining response, but serves as a comparison to the undrained response for which this approximation is very good. There are significant differences between the two responses, particularly the length scales over which the interaction takes place, and the generation of pore pressure in the saturated sand. Illustrations are presented to exhibit the effects of varying the applied pulse shape, and in particular the influence of the time scale of unloading relative to that of the loading.

2. THE COMPACTION MODEL

A granular material is a matrix composed of solid grains with inter-granular pore space filled with air (or other gas) or liquid. It is assumed here that the strains of both grains and matrix remain infinitesimal, so the relative pore volume change is also infinitesimal. The soil mechanics convention that strain and stress are measured positive in compression is adopted, so that positive normal components imply contraction of line elements and compressive force respectively. During shearing, the granular structure is rearranged and the pore volume decreases, causing compaction which is irreversible. In addition, part of the shear strain of the matrix is an irreversible shear settlement. Both the volume compaction and shear settlement will be described together as compaction for simplicity. The matrix strain $\boldsymbol{\varepsilon}$ is constructed as a sum of elastic and compaction strains $\boldsymbol{\varepsilon}^{\mathrm{e}}$ and $\boldsymbol{\varepsilon}^{\mathrm{c}}$ respectively, thus

$$\boldsymbol{\varepsilon} = \boldsymbol{\varepsilon}^{\mathrm{e}} + \boldsymbol{\varepsilon}^{\mathrm{c}} \tag{1}$$

where the elastic strains will be related to stress by hypoelastic laws, and the compaction strains will be determined by evolutionary differential relations. Hypoelasticity is path dependent, and so not reversible in general, but the compaction evolution is a distinct irreversible mechanism. The term elastic strain is used for simplicity. It is also convenient to partition the strain into a deviatoric part $\hat{\boldsymbol{\varepsilon}}$ and a compression part ε:

$$\boldsymbol{\varepsilon} = \hat{\boldsymbol{\varepsilon}} + \tfrac{1}{3}\varepsilon\mathbf{I}, \qquad \varepsilon = \mathrm{tr}(\boldsymbol{\varepsilon}) = \varepsilon^{\mathrm{e}} + \varepsilon^{\mathrm{c}} \tag{2}$$

with analogous partitions for the elastic and compaction strains

$$\boldsymbol{\varepsilon}^{\mathrm{e}} = \hat{\boldsymbol{\varepsilon}}^{\mathrm{e}} + \tfrac{1}{3}\varepsilon^{\mathrm{e}}\mathbf{I}, \qquad \boldsymbol{\varepsilon}^{\mathrm{c}} = \hat{\boldsymbol{\varepsilon}}^{\mathrm{c}} + \tfrac{1}{3}\varepsilon^{\mathrm{c}}\mathbf{I} \tag{3}$$

The corresponding partition of the stress $\boldsymbol{\sigma}$ into a deviatoric stress $\hat{\boldsymbol{\sigma}}$ and a mean pressure p is

$$\boldsymbol{\sigma} = \hat{\boldsymbol{\sigma}} + p\mathbf{I}, \qquad p = \tfrac{1}{3}\mathrm{tr}(\boldsymbol{\sigma}) \tag{4}$$

The total pressure p can be decomposed into partial pressures p^{s} in the matrix and p^{f} in the pore fluid:

$$p = p^{\mathrm{s}} + p^{\mathrm{f}} \tag{5}$$

The above partial pressures are related to the corresponding intrinsic pressure—the actual pressure $p^{\mathrm{s}}*$ supported by the grains and the fluid pore pressure $p^{\mathrm{f}}*$ respectively—by

$$p^{\mathrm{s}} = (1-\phi)p^{\mathrm{s}}*, \qquad p^{\mathrm{f}} = \phi p^{\mathrm{f}}* \tag{6}$$

where ϕ is the porosity of the medium, defined as the volume fraction of pore space in the matrix. It is assumed that the matrix supports the shear stress, with the viscous shear stress in the fluid negligible by comparison, and hence the partial stress in the fluid is isotropic pressure and the partial deviatoric stress in the solid is the total deviatoric stress.

As a unit volume of matrix compresses to a volume $1-\varepsilon$, the contained volume of solid $(1-\phi_0)$, with ϕ_0 being initial porosity, compresses to $(1-\phi)(1-\varepsilon)$, which is given by $(1-\phi_0)(1-\varepsilon^{\mathrm{I}})$, where ε^{I} is the intrinsic solid compression. Thus the porosity decrease is

$$\phi_0 - \phi = (1-\phi_0)(\varepsilon - \varepsilon^{\mathrm{I}}) = (1-\phi_0)(\varepsilon^{\mathrm{e}} - \varepsilon^{\mathrm{I}} + \varepsilon^{\mathrm{c}}) \tag{7}$$

That is, assuming that the grains strain purely elastically, it is the sum of the reversible change $(1-\phi_0)(\varepsilon^{\mathrm{e}}-\varepsilon^{\mathrm{I}})$ and the irreversible change $(1-\phi_0)\varepsilon^{\mathrm{c}}$. The elastic change in the pore volume can be expressed in the form

$$(1-\phi_0)(\varepsilon^{\mathrm{e}}-\varepsilon^{\mathrm{I}}) = \alpha_1 p^{\mathrm{s}} - \alpha_2 p^{\mathrm{f}} \tag{8}$$

where α_1 and α_2 are elastic constants which can be defined in terms of free draining and undrained compressibilities κ and $\bar{\delta}$, respectively, given by tests in isotropic pressure when no compaction occurs. Free draining conditions are then defined by

$$p^{\mathrm{f}} = 0, \quad p^{\mathrm{s}} = p, \quad \varepsilon = \varepsilon^{\mathrm{e}} = \kappa p, \quad \varepsilon^{\mathrm{I}} = \kappa_{\mathrm{s}} p^{\mathrm{s}*} \tag{9}$$

and undrained conditions are described by

$$\varepsilon = \varepsilon^{\mathrm{e}} = \bar{\delta} p, \quad \varepsilon = \kappa_{\mathrm{s}} p^{\mathrm{s}} + \kappa_{\mathrm{f}} p^{\mathrm{f}} \tag{10}$$

where the first relation in (10) holds only if there is no compaction ($\varepsilon^{\mathrm{c}} = 0$), while the second of (10) is also valid when compaction occurs. Substituting (9) and (10) into (8), and using (5) and (6), gives the expressions

$$\alpha_1 = (1-\phi_0)\kappa - \kappa_{\mathrm{s}}, \qquad (\bar{\delta}-\kappa_{\mathrm{s}})\alpha_2 = (1-\phi_0)(\kappa\kappa_{\mathrm{f}} + \bar{\delta}\kappa_{\mathrm{s}} - \bar{\delta}\kappa_{\mathrm{f}} - \bar{\delta}\kappa) \tag{11}$$

As an irreversible compression ($\varepsilon^{\mathrm{c}} > 0$) occurs in undrained conditions, from (7), (8) and $(10)_2$ it follows that

$$(1-\phi_0)\kappa_{\mathrm{f}} p^{\mathrm{f}} - \phi_0 \kappa_{\mathrm{s}} p^{\mathrm{s}} = \alpha_1 p^{\mathrm{s}} - \alpha_2 p^{\mathrm{f}} + (1-\phi_0)\varepsilon^{\mathrm{c}} \tag{12}$$

Substituting the definitions (11) into (12), and using (5), gives

$$p^{\mathrm{f}} = \eta(p + B\varepsilon^{\mathrm{c}}) \qquad \eta = \frac{\bar{\delta}-\kappa_{\mathrm{s}}}{\kappa_{\mathrm{f}}-\kappa_{\mathrm{s}}}, \qquad B = \frac{1}{\kappa-\kappa_{\mathrm{s}}} \tag{13}$$

and

$$\varepsilon^{\mathrm{e}} = \bar{\delta} p - \frac{\kappa-\bar{\delta}}{\kappa-\kappa_{\mathrm{s}}}\varepsilon^{\mathrm{c}} \tag{14}$$

and therefore a total compression relation

$$\varepsilon = \varepsilon^{\mathrm{e}} + \varepsilon^{\mathrm{c}} = \bar{\delta} p + A\varepsilon^{\mathrm{c}}, \qquad A = \frac{\bar{\delta}-\kappa_{\mathrm{s}}}{\kappa-\kappa_{\mathrm{s}}} \tag{15}$$

While the reversible undrained compressibility relation $(10)_1$ is recovered when ε^{c} is zero, the reversible dependence of ε^{e} on p^{s} and p^{f} does not reduce simply to proportionality to p with factor $\bar{\delta}$ when ε^{c} is not zero. The undrained limit is an appropriate approximation for wave propagation analysis in which transient time scales are too short for significant drainage, and must also yield the maximum pore pressures since no squeezing out of the fluid is permitted. The pore pressure $p^{\mathrm{f}}*$ is given by (13) with the relation $(6)_2$, but also of concern in the compaction model is the effective pressure defined by

$$\bar{p} = p - p^{\mathrm{f}}* = \left(1 - \frac{\eta}{\phi_0}\right)p - \frac{\eta B}{\phi_0}\varepsilon^{\mathrm{c}} \tag{16}$$

which is a measure of the inter-granular contact pressure which influences the shearing response.

Now in a dry matrix with highly compressible pore gas, $\kappa_f \gg (\kappa_s, \bar{\delta})$, and supposing that $\varepsilon^c \not\gg \varepsilon^e$, then, from (13) $p^f \approx 0$ in comparison with p. That is, the undrained limit, and hence intermediate cases, approach the free draining limit with $p^f = 0$, $p^s = p$ and $\bar{\delta} = \kappa$, and the explicit relations (9) apply, involving only the two compressibilities κ and κ_s. The latter only enters the expressions for pore volume change and the intrinsic grain strain. The dry matrix model is described directly in terms of the compressions ε^e and ε^c, and κ_s does not appear. An incompressible grain approximation, $\kappa_s = 0$, therefore offers no further simplification for the dry matrix. For the liquid saturated matrix in undrained conditions, the approximation $\kappa_s = 0$ corresponding to $\kappa_s \ll (\bar{\delta}, \kappa_f)$ leads to

$$\eta = \frac{\bar{\delta}}{\kappa_f}, \qquad B = \frac{1}{\kappa}, \quad A = \frac{\bar{\delta}}{\kappa} \tag{17}$$

With this approximation,

$$\bar{p} = \frac{\phi_0 \kappa_f - \bar{\delta}}{\phi_0 \kappa_f} p - \frac{\bar{\delta}}{\phi_0 \kappa_f \kappa} \varepsilon^c \tag{18}$$

which then suggests that

$$\phi_0 \kappa_f > \bar{\delta} \tag{19}$$

if the effective pressure is not to become negative (less than the atmospheric pressure adopted as the zero state) immediately compaction takes place*. The weak inequality of (19) was deduced by Morland[13]; however, the equality is a common soil mechanics assumption.

A variable ξ which is strictly increasing as shearing takes place, but remains constant during purely isotropic straining, is introduced to map the evolution of shear strain as the material is stressed. This loading parameter is time independent. In the selected model from Morland, *et al.*[12] it is defined by

$$\mathrm{d}\xi = \sqrt{\{\tfrac{1}{2}\mathrm{tr}[(\mathrm{d}\hat{\boldsymbol{\varepsilon}})^2]\}} \tag{20}$$

which represents accumulating deviatoric strain. The elastic compression is determined by one of the previous free-draining or undrained relations $(9)_3$ or (14) respectively, which in rate form become

$$\frac{\mathrm{d}\varepsilon^e}{\mathrm{d}\xi} = \kappa \frac{\mathrm{d}p}{\mathrm{d}\xi}, \qquad \text{or} \qquad \frac{\mathrm{d}\varepsilon^e}{\mathrm{d}\xi} = \bar{\delta} \frac{\mathrm{d}p}{\mathrm{d}\xi} - \left(\frac{\kappa - \bar{\delta}}{\kappa - \kappa_s} \right) \frac{\mathrm{d}\varepsilon^c}{\mathrm{d}\xi} \tag{21}$$

though the rate form does not apply during purely isotropic straining when ξ remains constant. The elastic shear strains are governed by a hypoelastic shear law

$$2G(\bar{p}) \frac{\mathrm{d}\hat{\boldsymbol{\varepsilon}}^e}{\mathrm{d}\xi} = \frac{\mathrm{d}\hat{\boldsymbol{\sigma}}}{\mathrm{d}\xi} \tag{22}$$

* A referee has pointed out that negative pressure can occur due to internal flows, observed experimentally by Mokni[14], and numerically simulated by Schrefler *et al.*[15]. In our later illustrations, $\bar{\delta}$ is chosen to satisfy (19), and would therefore exclude possible local negative pressures.

where the shear modulus $G(\bar{p})$ is a matrix property which is assumed here to depend on the current state through the effective pressure $\bar{p}$. This law also determines the total shear response when the material is fully compacted and no further pore collapse takes place.

The compaction ε^c and irreversible shear strain $\hat{\boldsymbol{\varepsilon}}^c$ are governed by evolution laws. Define

$$\psi = \tfrac{1}{2}\mathrm{tr}[(\hat{\boldsymbol{\varepsilon}})^2] \tag{23}$$

which is a positive current deviatoric state measure on which the rates are assumed to depend, then the adopted model laws[11] are

$$\frac{\mathrm{d}\varepsilon^c}{\mathrm{d}\xi} = D = \sqrt{3}(\bar{a}R(\varepsilon^c)H(\psi)) \tag{24}$$

$$\frac{\mathrm{d}\hat{\boldsymbol{\varepsilon}}^c}{\mathrm{d}\xi} = T\hat{\boldsymbol{\varepsilon}} = R(\varepsilon^c)H(\psi)S(\psi)\psi^{-1/2}\hat{\boldsymbol{\varepsilon}} \tag{25}$$

where in the separable forms the functions $R(\varepsilon^c)$, $H(\psi)$ and $S(\psi)$ are dimensionless, positive and normalized by

$$R(0) = H(0) = S(0) = 1 \tag{26}$$

and $\bar{a}$ is a positive constant satisfying

$$0 < \bar{a} < 1 \tag{27}$$

Thus,

$$D \geqslant 0, \qquad T \geqslant 0 \tag{28}$$

so that dilatancy does not occur, and $\hat{\boldsymbol{\varepsilon}}$ defines the direction of the shear compaction rate. A common decay $R(\varepsilon^c)$ with compaction seems sensible, though not necessary, and the extra factor $S(\psi)$ is introduced in (25) to retain a common factor $\mathrm{H}(\psi)$ in both laws.

The selected method (B) from Morland *et al.*[12] was correlated with uni-axial load–unload data to an axial stress $1{\cdot}17 \times 10^6$ Pa for a loose dry sand of initial porosity $\phi_0 = 0{\cdot}41$, determining the constants κ and a, and the functions $G(p)$, $R(\varepsilon^c)$, $H(\psi)$ and $S(\psi)$ in the forms

$$\begin{aligned} R(\varepsilon^c) &= \exp\left\{ -\sum_{n=1}^{5} r_n \left(\frac{\varepsilon^c}{\varepsilon^*}\right)^n \right\}, \qquad \bar{H}(\varepsilon_z) = 1 + \sum_{n=1}^{5} h_n \left(\frac{\varepsilon_z}{\varepsilon^*}\right)^n \\ g(p) &= g_0 + \sum_{n=1}^{5} g_n \left(\frac{p}{p^*}\right)^n, \qquad \bar{S}(\varepsilon_z) = 1 + \sum_{n=1}^{5} s_n \left(\frac{\varepsilon_z}{\varepsilon^*}\right)^n \end{aligned} \tag{29}$$

where

$$H(\psi) = \bar{H}(\sqrt{(3\psi)}), \quad S(\psi) = \bar{S}(\sqrt{(3\psi)}), \quad g(p) = \tfrac{2}{3}\kappa G(p), \quad g_0 = g(0) \tag{30}$$

and the normalizing stress and strain units are

$$p^* = 1 \times 10^6 \text{ Pa}, \qquad \varepsilon^* = 0{\cdot}01 \tag{31}$$

Table I. Model coefficients

n	r_n	h_n	s_n	g_n
1	0·9850	0·2711	0·5667	0·7169
2	0·8938	0·5731	− 4·9571	− 0·1924
3	1·3061	0·4299	3·7706	0·0564
4	1·1841	0·7044	3·3436	− 0·0004
5	0·8597	0·8735	− 2·7056	0·0014

p becomes $\bar{p}$ in the shear law for the liquid saturated matrix. The coefficients shown in Table I correct those given in error for an alternative $g(p)$ construction and the associated parameters are

$$\phi_0 = 0{\cdot}41, \quad \bar{a} = 0{\cdot}8957, \quad g_0 = 0{\cdot}0341, \quad \kappa = 0{\cdot}62 \times 10^{-8}\ \mathrm{Pa}^{-1}, \quad G_0^p = 8{\cdot}25 \times 10^6\ \mathrm{Pa} \tag{32}$$

Combining the compaction relations (24) and (25) with the elastic relations in rate form, (21) and (22), provides an evolutionary law for the total strain $\boldsymbol{\varepsilon}$ in terms of the loading parameter ψ defined by (23).

3. UNI-AXIAL MOTION

The waves induced by the applied stress at the surface are assumed to be plane and restricted to uni-axial motion. This is a reasonable approximation for near surface behaviour over a central zone during several pulse times if the stress is applied uniformly over an area with dimensions large relative to the pulse length, while disturbances from the loading edge have not penetrated. Dynamic compaction will exhibit its major influence in such near-surface regions before significant attenuation occurs. The total strain is therefore uni-axial, but the elastic and compaction parts will have cancelling non-zero lateral components.

Let $Oxyz$ be rectangular Cartesian axes and consider uni-axial strain ε_z in the Oz direction induced by an axial compressive stress σ_z, with responsive compressive lateral stresses $\sigma_x = \sigma_y$ to maintain the lateral constraints $\varepsilon_x = \varepsilon_y = 0$. The stress and strain tensors therefore have the forms

$$\boldsymbol{\sigma} = \begin{pmatrix} \sigma_x & 0 & 0 \\ 0 & \sigma_x & 0 \\ 0 & 0 & \sigma_z \end{pmatrix}, \qquad \boldsymbol{\varepsilon} = \begin{pmatrix} 0 & 0 & 0 \\ 0 & 0 & 0 \\ 0 & 0 & \varepsilon_z \end{pmatrix} \tag{33}$$

with associated deviatoric stress and strain tensors

$$\hat{\boldsymbol{\sigma}} = \frac{1}{3}\begin{pmatrix} \sigma_x - \sigma_z & 0 & 0 \\ 0 & \sigma_x - \sigma_z & 0 \\ 0 & 0 & 2(\sigma_z - \sigma_x) \end{pmatrix} \tag{34}$$

$$\hat{\boldsymbol{\varepsilon}} = \frac{1}{3}\begin{pmatrix} -\varepsilon_z & 0 & 0 \\ 0 & -\varepsilon_z & 0 \\ 0 & 0 & 2\varepsilon_z \end{pmatrix} \tag{35}$$

The elastic and compaction strain tensors $\boldsymbol{\varepsilon}^{\mathrm{e}}$ and $\boldsymbol{\varepsilon}^{\mathrm{c}}$ have non-zero lateral components, and have analogous forms to $\boldsymbol{\sigma}$, while the deviatoric tensors $\hat{\boldsymbol{\varepsilon}}^{\mathrm{e}}$ and $\hat{\boldsymbol{\varepsilon}}^{\mathrm{c}}$ have analogous forms to $\hat{\boldsymbol{\sigma}}$. The loading parameter ξ defined by (20) becomes

$$\mathrm{d}\xi = (-1)^n 3^{-1/2}\,\mathrm{d}\varepsilon_z \tag{36}$$

where $n = 0$ during loading (increasing ε_z) and $n = 1$ during unloading (decreasing ε_z), or alternatively n even and odd respectively during loading and unloading. It will be inferred that loading and unloading also correspond to σ_z increasing and decreasing respectively. The state parameter ψ defined by (23) becomes

$$\psi = \tfrac{1}{3}(\varepsilon_z)^2 \tag{37}$$

and hence the argument $\sqrt{(3\psi)}$ of $\bar{H}$ and $\bar{S}$ in the model (29) is simply ε_z given that ε_z remains non-negative during the motion.

The free draining and undrained relations for the total compression strain increment, combining (21) and (24), can be expressed in the common form

$$(\mathrm{d}\sigma_z + 2\mathrm{d}\sigma_x) = 3\Omega(d\varepsilon_z - \omega D\,\mathrm{d}\xi) \tag{38}$$

where

$$\text{free:}\quad \Omega = 1/\kappa,\quad \omega = 1;\quad \text{undrained:}\quad \Omega = 1/\bar{\delta},\quad \omega = A \tag{39}$$

The deviatoric relations (22) and (25) combine to give

$$(\mathrm{d}\sigma_z - \mathrm{d}\sigma_x) = 2G(\mathrm{d}\varepsilon_z - T\varepsilon_z\,\mathrm{d}\xi) \tag{40}$$

Eliminating $\mathrm{d}\sigma_x$, and expressing $\mathrm{d}\xi$ in terms of $\mathrm{d}\varepsilon_z$ by (36), gives the total stress–strain slopes

$$\frac{\mathrm{d}\sigma_z}{\mathrm{d}\varepsilon_z} = \Omega + \frac{4}{3}G - (-1)^n 3^{-1/2}\left(\Omega\omega D + \frac{4}{3}GT\varepsilon_z\right) \tag{41}$$

with n even and odd defining loading and unloading respectively. The model correlation[12] has both slopes positive, so that loading and unloading correspond to both ε_z and σ_z increasing or decreasing respectively. With the expression (39), and decompositions (24) and (25) with dependencies (29), the explicit relations for free and undrained motion are respectively

$$\text{free:}\quad \kappa\frac{\mathrm{d}\sigma_z}{\mathrm{d}\varepsilon_z} = 1 + 2g(p) - (-1)^n R(\varepsilon^{\mathrm{c}})\bar{H}(\varepsilon_z)\{\bar{a} + 2g(p)\bar{S}(\varepsilon_z)\} \tag{42}$$

$$\text{undrained:}\quad \kappa\frac{\mathrm{d}\sigma_z}{\mathrm{d}\varepsilon_z} = \frac{\kappa}{\bar{\delta}} + 2g(\bar{p}) - (-1)^n R(\varepsilon^{\mathrm{c}})\bar{H}(\varepsilon_z)\left\{\frac{\kappa}{\bar{\delta}}A\bar{a} + 2g(\bar{p})\bar{S}(\varepsilon_z)\right\} \tag{43}$$

where the function arguments ε^{c}, defined by (24), and $\bar{p}$ defined by (16) and (38) with (39), are given by the evolution equations

$$\frac{\mathrm{d}\varepsilon^{\mathrm{c}}}{\mathrm{d}\varepsilon_z} = (-1)^n \bar{a} R(\varepsilon^{\mathrm{c}})\bar{H}(\varepsilon_z) \tag{44}$$

$$\frac{\mathrm{d}\bar{p}}{\mathrm{d}\varepsilon_z} = \frac{1}{\bar{\delta}}\left(1 - \frac{\eta}{\phi_0}\right) - \left\{\frac{A}{\bar{\delta}}\left(1 - \frac{\eta}{\phi_0}\right) + \frac{\eta B}{\phi_0}\right\}\frac{\mathrm{d}\varepsilon^{\mathrm{c}}}{\mathrm{d}\varepsilon_z} \tag{45}$$

The relations (42) and (44) are two simultaneous differential equations for the evolution of ε_z and ε^c in the free draining as σ_z is varied, distinguishing increasing and decreasing σ_z by even and odd n respectively, but can also be solved for σ_z when ε_z is varied. For undrained conditions there are three simultaneous differential equations (43), (44) and (45) for the evolution of ε_z, ε^c and $\bar{p}$. With the incompressible grain approximation $\kappa_s = 0$ for which the expressions (17) and (18) hold, the axial stress–strain slope (43) for undrained conditions becomes

$$\text{undrained:} \quad \kappa \frac{\mathrm{d}\sigma_z}{\mathrm{d}\varepsilon_z} = \frac{\kappa}{\bar{\delta}} + 2g(\bar{p}) - (-1)^n R(\varepsilon^c)\bar{H}(\varepsilon_z)\{\bar{a} + 2g(\bar{p})\bar{S}(\varepsilon_z)\} \tag{46}$$

and the effective pressure equation (45) simplifies to

$$\frac{\mathrm{d}\bar{p}}{\mathrm{d}\varepsilon_z} = \frac{\phi_0 \kappa_f - \bar{\delta}}{\phi_0 \kappa_f \bar{\delta}} - \frac{1}{\kappa}\frac{\mathrm{d}\varepsilon^c}{\mathrm{d}\varepsilon_z} \tag{47}$$

and the compaction equation (44) is unchanged. The free draining stress–strain slope (42) is also unchanged.

The free draining differential equations (42) and (44) were solved by Morland *et al.*[12] for load–unload cycles of axial stress to a sequence of maximum stresses up to $1{\cdot}17 \times 10^6$ Pa, each following the same loading path in the ε_z–σ_z plane, to the respective maximum stress, but unloading along different paths from the respective maximum stress points. However, it was discovered that to a good approximation, the unloading paths had a common shape which was translated parallel to the strain axis; that is, the stress–strain slope depends only on σ_z and is common to all unloading curves. Thus in any region in which successive material elements unload from different stress levels due to attenuation of a preceding loading wave, the stress–strain slope, and hence also characteristic slope and the wave speed, is a common function of σ_z for all particles. The loading and common unloading path slopes for model (B) are respectively

loading

$$\frac{\varepsilon^*}{p^*}\frac{\mathrm{d}\sigma_z}{\mathrm{d}\varepsilon_z} = 0{\cdot}1043 + 4{\cdot}8343\left(\frac{\sigma_z}{p^*}\right) - 11{\cdot}3184\left(\frac{\sigma_z}{p^*}\right)^2 + 20{\cdot}8670\left(\frac{\sigma_z}{p^*}\right)^3 - 26{\cdot}6914\left(\frac{\sigma_z}{p^*}\right)^4 + 18{\cdot}6708\left(\frac{\sigma_z}{p^*}\right)^5 - 5{\cdot}0146\left(\frac{\sigma_z}{p^*}\right)^6 \tag{48}$$

unloading

$$\frac{\varepsilon^*}{p^*}\frac{\mathrm{d}\sigma_z}{\mathrm{d}\varepsilon_z} = 1{\cdot}9125 + 2{\cdot}2933\left(\frac{\sigma_z}{p^*}\right) - 0{\cdot}4784\left(\frac{\sigma_z}{p^*}\right)^2 + 0{\cdot}4495\left(\frac{\sigma_z}{p^*}\right)^3 \tag{49}$$

where the normalizing stress and strain units p^* and ε^* are defined by (31). From zero stress to 10^6 Pa the loading slope increases from 0·104 to $1{\cdot}452 \times 10^8$ Pa, and the unloading slope from 1·913 to $4{\cdot}177 \times 10^8$ Pa, which are far from uniform slopes, but for a simple wave analysis to compare free draining results with those of undrained results, separate constant slopes and wave speeds will be assumed. For illustration the following constant mean values are adopted for the

free draining response:

loading

$$\frac{\mathrm{d}\sigma_z}{\mathrm{d}\varepsilon_z} = 0{\cdot}72 \times 10^8 \text{ Pa};$$

unloading

$$\frac{\mathrm{d}\sigma_z}{\mathrm{d}\varepsilon_z} = 2{\cdot}88 \times 10^8 \text{ Pa} \tag{50}$$

Since the positive loading and unloading slopes defined by (42) for free draining are quite different, both the common term and that changing sign with n have similar magnitudes, and the non-uniformity arises through all the functions $g(p)$, $R(\varepsilon^c)$, $\bar{H}(\varepsilon_z)$, $\bar{S}(\varepsilon_z)$. Turning to the undrained slope (46) for incompressible grains which will be used for illustrations, then since

$$\bar{\delta} < \phi_0 \kappa_f = 0{\cdot}21 \times 10^{-9} \text{ Pa} < \kappa = 0{\cdot}62 \times 10^{-8} \text{ Pa}^{-1} \tag{51}$$

when the pore fluid is water with $\kappa_f = 0{\cdot}51 \times 10^{-9}$ Pa^{-1}, the constant term $(\kappa/\bar{\delta}) > 29{\cdot}5$ dominates both loading and unloading slopes, which are therefore much closer in magnitude and will each be approximately uniform since the varying function contributions are now relatively small. This dominance and consequences follow also for the general slope (43). For illustration and applications the following compressibilities are adopted with the undrained slope relation (46):

$$\kappa_f = 0{\cdot}51 \times 10^{-9} \text{ Pa}^{-1}, \quad \kappa = 0{\cdot}62 \times 10^{-8} \text{ Pa}^{-1}, \quad \bar{\delta} = 0{\cdot}2 \times 10^{-9} \text{ Pa}^{-1}, \quad (\kappa/\bar{\delta}) = 31 \tag{52}$$

Figure 1 shows the corresponding stress–strain paths for a sequence of load–unload cycles to different maximum stresses up to $1{\cdot}17 \times 10^6$ Pa, which demonstrate the near uniformity of the

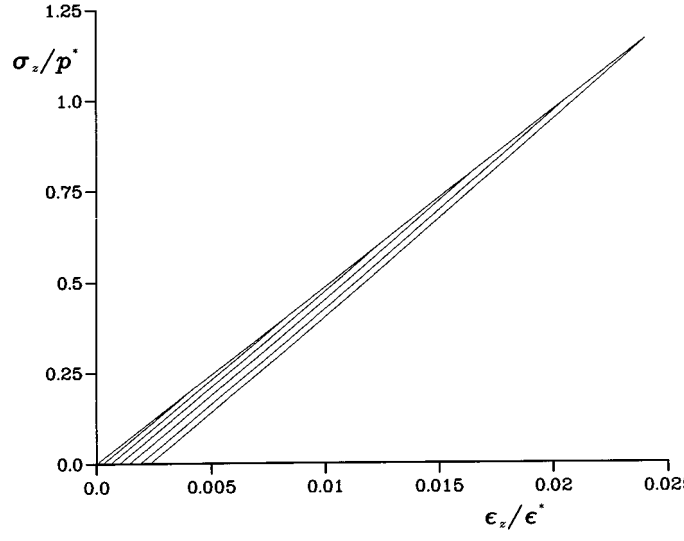

Figure 1. Stress–strain paths for load–unload cycles

loading slope and common unloading slope, and the calculated paths determine the approximate constant slope values for undrained response:

loading

$$\frac{\mathrm{d}\sigma_z}{\mathrm{d}\varepsilon_z} = 4{\cdot}86 \times 10^9 \text{ Pa}$$

unloading

$$\frac{\mathrm{d}\sigma_z}{\mathrm{d}\varepsilon_z} = 5{\cdot}38 \times 10^9 \text{ Pa} \tag{53}$$

The constant free draining slopes (50) and constant undrained slopes (53) are adopted for the subsequent wave propagation applications. The compaction ε^{c} must be calculated, however, from the evolution equation (44) which gives a common $\varepsilon^{\mathrm{c}}(\varepsilon_z)$ for both free and undrained response, but different variation with σ_z according to which of the stress–strain relations (50) and (53) is followed. The pore pressure evolution in the undrained response is determined by (13) and (15) with $\varepsilon = \varepsilon_z$ in uni-axial motion; thus

$$\frac{\mathrm{d}p^{\mathrm{f}}*}{d\varepsilon_z} = \frac{\eta}{\phi_0 \bar{\delta}} \left\{ 1 + (\bar{\delta} B - A) \frac{\mathrm{d}\varepsilon^{\mathrm{c}}}{\mathrm{d}\varepsilon_z} \right\} \tag{54}$$

which simplifies to

$$\frac{\mathrm{d}p^{\mathrm{f}}*}{\mathrm{d}\varepsilon_z} = \frac{1}{\phi_0 \kappa_{\mathrm{f}}} \tag{55}$$

with the incompressible grain approximations (17) which are adopted in the applications.

4. WAVE PROPAGATION

With an infinitesimal strain and displacement approximation, and in the absence of body force, the uni-axial momentum equation is

$$\frac{\partial \sigma_z}{\partial z} = -\rho \frac{\partial v}{\partial t} \tag{56}$$

where t denotes time and v is the axial velocity of the matrix in free draining motion in which the inertia of the gas is neglected, and is the common velocity of grains and liquid in undrained motion. Recall that here stress is measured positive in compression. ρ is the mixture density given by

$$\rho = \rho^{\mathrm{s}} + \rho^{\mathrm{f}}, \quad \rho^{\mathrm{s}} = (1 - \phi_0)\rho^{\mathrm{s}}*, \quad \rho^{\mathrm{f}} = \phi_0 \rho^{\mathrm{f}}* \tag{57}$$

where ρ^{s} and $\rho^{\mathrm{s}}*$ are the partial and intrinsic grain densities, and ρ^{f} and $\rho^{\mathrm{f}}*$ are the partial and intrinsic fluid densities. For free draining the gas density is neglected by comparison with the grain density, so that

free

$$\rho = \rho^{\mathrm{s}} = (1 - \phi_0)\rho^{\mathrm{s}}* \tag{58}$$

With intrinsic sand and water densities and porosity

$$\rho^{s*} = 2{\cdot}55 \times 10^3 \text{ kg m}^{-3}, \quad \rho^{f*} = 1{\cdot}0 \times 10^3 \text{ kg m}^{-3}, \quad \phi_0 = 0{\cdot}41 \tag{59}$$

the mixture densities are

free

$$\rho = 1{\cdot}5 \times 10^3 \text{ kg m}^{-3},$$

undrained

$$\rho = 1{\cdot}9 \times 10^3 \text{ kg m}^{-3} \tag{60}$$

The axial velocity v is related to the compressive strain ε_z by

$$\frac{\partial v}{\partial z} = -\frac{\partial \varepsilon_z}{\partial t} \tag{61}$$

A stress–strain relation of a form $\sigma_z = \sigma_z(\varepsilon_z, z)$ applies to both loading and unloading particles z in free draining and undrained response, with the explicit z dependence required when unloading occurs on paths from different maximum stresses, and with the model approximations that the stress–strain slopes are constant in both loading and unloading regions, crude for free draining but excellent for undrained response, then

loading

$$\frac{\partial \sigma_z}{\partial \varepsilon_z} = \rho c_l^2,$$

unloading

$$\frac{\partial \sigma_z}{\partial \varepsilon_z} = \rho c_u^2 \tag{62}$$

where c_l and c_u are distinct constants, with different pairs for free draining and undrained response. Thus

$$\frac{\partial \sigma_z}{\partial t} = \frac{\partial \sigma_z}{\partial \varepsilon_z}\frac{\partial \varepsilon_z}{\partial t}, \qquad \frac{\partial^2 \sigma_z}{\partial t^2} = \rho c^2 \frac{\partial^2 \varepsilon_z}{\partial t^2} \tag{63}$$

Eliminating v between (56) and (61), then ε_z by (63), shows that σ_z satisfies a wave equation

$$c^2 \frac{\partial^2 \sigma_z}{\partial z^2} = \frac{\partial^2 \sigma_z}{\partial t^2} \tag{64}$$

with a constant wave speed c which is c_l or c_u respectively in loading and unloading regions. For the constant stress–strain slopes (50) for free draining and (53) for undrained response, with corresponding ρ given by (60), the respective wave speeds are

free

$$c_l = 2{\cdot}2 \times 10^2 \text{ m s}^{-1}, \qquad c_u = 4{\cdot}4 \times 10^2 \text{ m s}^{-1} \tag{65}$$

undrained

$$c_l = 1{\cdot}6 \times 10^3 \text{ m s}^{-1}, \qquad c_u = 1{\cdot}68 \times 10^3 \text{ m s}^{-1} \tag{66}$$

Once the stress wave solution is determined, the strain ε_z is given by (62), and the compaction ε^c is then calculated by (44) for both free draining and undrained conditions, and the pore pressure p^{f*} for undrained conditions by (55).

The time scale of the stress variation is governed by that of the applied surface pulse, t^* say, and the corresponding length scale z^* is that of a wave, say an unloading wave. Introduce normalized dimensionless co-ordinates (Z, T) by

$$t = t^* T, \qquad z = z^* Z, \qquad z^* = c_u t^* \tag{67}$$

and normalized dimensionless stress, strain and particle velocity Σ, E and V by

$$(\sigma_z, p^{f*}) = p^f(\Sigma, P^{f*}), \qquad (\varepsilon_z, \varepsilon^c) = \ = \varepsilon^*(E, E^c), \qquad v = \varepsilon^* c_u V \tag{68}$$

and define the ratio of the loading and unloading wave speeds by

$$\gamma = c_l / c_u < 1 \tag{69}$$

The lengths scales z^* and ratios γ are different for free draining and undrained conditions:

free

$$z^* = 4{\cdot}4 \times 10^2 \text{ m s}^{-1} t^*, \qquad \gamma = 0{\cdot}5$$

undrained

$$z^* = 1{\cdot}68 \times 10^3 \text{ m s}^{-1} t^*, \qquad \gamma = 0{\cdot}95 \tag{70}$$

Loading and unloading are now governed by the normalized stress wave equations

loading

$$\gamma^2 \frac{\partial^2 \Sigma}{\partial Z^2} = \frac{\partial^2 \Sigma}{\partial T^2}$$

unloading

$$\frac{\partial^2 \Sigma}{\partial Z^2} = \frac{\partial^2 \Sigma}{\partial T^2} \tag{71}$$

with normalized wave speeds γ and unity respectively. The strains at a fixed Z are determined by the strain–stress slopes

loading

$$\frac{\partial E}{\partial \Sigma} = \frac{k}{\gamma^2}$$

unloading

$$\frac{\partial E}{\partial \Sigma} = k \tag{72}$$

where

free

$$k = k_{\mathrm{f}} = \frac{p^*}{\rho c_{\mathrm{u}}^2 \varepsilon^*} = 0{\cdot}344$$

undrained

$$k = k_{\mathrm{u}} = \frac{p^*}{\rho c_{\mathrm{u}}^2 \varepsilon^*} = 0{\cdot}0186 \tag{73}$$

and the particle velocities from both (4·1) and (4·6) by

$$\frac{\partial V}{\partial T} = -k\frac{\partial \Sigma}{\partial Z}, \qquad \text{loading: } \frac{\partial V}{\partial Z} = -\frac{k}{\gamma^2}\frac{\partial \Sigma}{\partial T}, \quad \text{unloading: } \frac{\partial V}{\partial Z} = -k\frac{\partial \Sigma}{\partial T} \tag{74}$$

The compaction evolution (44) becomes

$$\frac{\mathrm{d}E^{\mathrm{c}}}{\mathrm{d}E} = (-1)^n \bar{a} R(\varepsilon^* E^{\mathrm{c}}) \bar{H}(\varepsilon^* E) \tag{75}$$

for both free draining and undrained conditions, but since the strain distribution in space and time for a given stress pulse will be very different for free draining and undrained conditions, the compaction evolution will also be very different. The pore pressure evolution (55) for undrained response becomes simply

$$\frac{\partial P^{\mathrm{f}*}}{\partial E} = 47{\cdot}82 \tag{76}$$

In comparison, by (72) with the undrained values of γ and k given by (70) and (73),

loading

$$\partial \Sigma / \partial E = 48{\cdot}52$$

unloading

$$\partial \Sigma / \partial E = 53{\cdot}76 \tag{77}$$

which are similar in magnitude to the slope (76). However, integration from the initial zero stress and pore pressure through a stress load–unload cycle leaves, in general, a residual pore pressure, which is shown in later illustrations.

Consider an applied continuous loading–unloading stress pulse on the surface $Z = 0$ of an infinite medium, for which the stress rises from zero to Σ_M at dimensionless time $T = \tau$, and decreases to zero at time $T = 1$ and then remains zero. Figure 2 illustrates the pattern of wave characteristics in a (Z, T) plane induced by such a pulse, including the continuous interface path $Z = S(T)$ propagating from the surface at time τ when unloading starts, which separates regions of increasing and decreasing stress governed by the respective loading and unloading wave equations. The interface stress attenuates as the faster unloading waves overtake and interact with the preceding loading wave, and there are reflected waves from the interface to

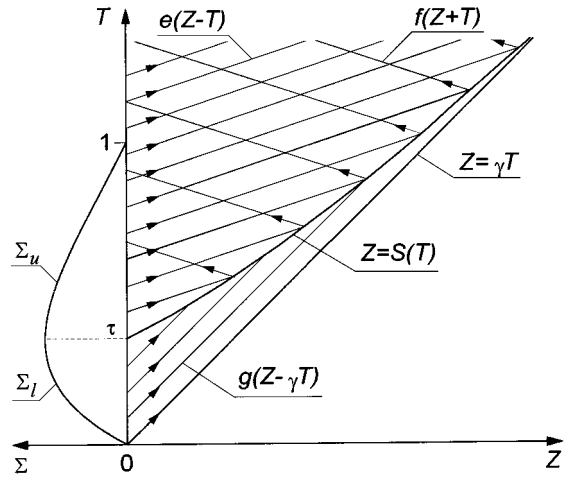

Figure 2. Wave characteristics pattern for a continuous load–unload pulse

maintain momentum balance. The region ahead of the loading front which propagates from the surface at time $T = 0$ is undisturbed. Since the signals reflected from the interface are loading, then, depending on the outgoing unloading wave profile, reloading may occur at some stage in the assumed unloading region when the solution would become invalid. Unloading must therefore be tested to determine how far the assumed wave pattern is valid. There is no general analytic result, but in present applications the pattern remains valid long enough for the major propagation features to develop. This situation is analogous to the interaction of elastic and plastic uni-axial waves analysed by Morland[16] and in more detail for constant wave speeds by Morland and Cox[14]. It is convenient to extend the function $S(T)$ to define also the surface $Z = 0$ in $T < \tau$, and hence complete a boundary of the loading domain, thus

$$0 \leqslant T \leqslant \tau: \qquad S(T) = 0 \tag{78}$$

then the above pattern expressed in terms of wave function solutions of the linear wave equations (71) becomes

$$T > 0: \gamma T < Z: \Sigma = 0, \qquad S(T) < Z < \gamma T: \Sigma = g(Z - \gamma T) \tag{79}$$

$$T > \tau: 0 < Z < S(T): \Sigma = e(Z - T) + f(Z + T) \tag{80}$$

where the arguments $Z - \gamma T$ is negative in $Z < \gamma T$, and the argument $Z + T$ is positive in $T > \tau$. Since the interface overtakes the loading wave and is overtaken by the unloading wave,

$$T > \tau: \gamma < S'(T) < 1, \qquad \gamma(T - \tau) < S(T) < T - \tau \tag{81}$$

where $'(\ )$ denotes differentiation with respect to argument, then

$$T > \tau: Z - T < S - T < -\tau \tag{82}$$

and the argument $Z - T$ is negative in $T > \tau$. The associated particle velocity distributions given by integrating both derivatives in (74) are

$$\gamma T < Z\colon V = 0, \qquad S(T) < Z < \gamma T\colon V = \frac{k}{\gamma} g(Z - \gamma T) \tag{83}$$

$$0 < Z < S(T)\colon V = k[e(Z - T) - f(Z + T)] \tag{84}$$

noting that both Σ and V vanish on $Z = \gamma T$.

The three wave functions $g(Z - \gamma T)$, $e(Z - T)$, $f(Z + T)$, and interface path $S(T)$, are determined by the prescribed increasing stress and prescribed decreasing stress on the sections of the surface $Z = 0$ bounding the loading and unloading domains respectively, together with continuity of stress and particle velocity on the interface $Z = S(T)$. That is, the prescribed surface stress gives

$$Z = 0\colon g(-\gamma T) = \Sigma_{\mathrm{l}}(T),\ 0 = < T < \tau; \qquad e(-T) + f(T) = \Sigma_{\mathrm{u}}(T),\ \tau < T \tag{85}$$

where $\Sigma_{\mathrm{l}}(T)$ and $\Sigma_{\mathrm{u}}(T)$ are the loading and unloading stress variations respectively, continuous at $T = \tau$, with $\Sigma_u(T)$ zero in $T > 1$. These determine $g(Z - \gamma T)$ for negative argument $Z - \gamma T$ as required in (79), and relate $e(-T)$ and $f(T)$ at negative and positive arguments respectively as required in (80). The interface stress and particle velocity continuity conditions give

$$Z = S(T)\colon\ g[S(T) - \gamma T] = e[S(T) - T] + f[S(T) + T], \quad \tau < T \tag{86}$$

$$Z = S(T)\colon\ g[S(T) - \gamma T] = \gamma\{e[S(T) - T] - f[S(T) + T]\}, \quad \tau < T \tag{87}$$

Now by (81) the argument $S(T) - T$ is a decreasing negative function of T, and the arguments $S(T) - \gamma T$ and $S(T) + T$ are increasing positive functions of T, so (86) and (87) relate functions with monotonically changing arguments as T increases, and with signs consistent with (85). Combining (85–87) and eliminating $e[S(T) - T]$ and $f[S(T) + T]$ in turn , gives the explicit expressions for $\tau < T$,

$$e[S(T) - T] = \frac{1 + \gamma}{2\gamma}\Sigma_{\mathrm{l}}[T - S(T)/\gamma], \qquad f[S(T) + T] = -\frac{1 - \gamma}{2\gamma}\Sigma_{\mathrm{l}}[T - S(T)/\gamma] \tag{88}$$

which, together with $(85)_2$, are three functional difference relations for the interface path $S(T)$ and unknown wave functions $e[S(T) - T]$ and $f[S(T) + T]$. Physically, (88) relate the outgoing and reflected waves in the unloading domain which intersect at the interface at time T, to the outgoing loading wave overtaken at time T, while $(85)_2$ relates those meeting at the surface to the applied stress there.

The three algebraic difference equations $(85)_2$ and (88) can be solved numerically by a time-stepping algorithm from $T = \tau$, starting from the known wave functions, interface speed and wave function derivatives evaluated at τ, which are obtained explicitly from (88) and the derivatives of the three equations:

$$-e'(-T) + f'(T) = \Sigma'_{\mathrm{u}}(T) \tag{89}$$

$$[1 - S'(T)]e'(-T) = \frac{1 + \gamma}{2\gamma^2}[S'(T) - \gamma]\Sigma'_{\mathrm{l}}(T) \tag{90}$$

$$[1 + S'(T)]f'(T) = \frac{1 - \gamma}{2\gamma^2}[S'(T) - \gamma]\Sigma'_{\mathrm{l}}(T) \tag{91}$$

Immediately from (88)

$$e(-\tau) = \frac{1+\gamma}{2\gamma}\Sigma_l(\tau), \qquad f(\tau) = -\frac{1-\gamma}{2\gamma}\Sigma_l(\tau) \tag{92}$$

First suppose that the loading–unloading change is abrupt, with neither $\Sigma_l'(\tau)$ nor $\Sigma_u'(\tau)$ zero, then

$$\Sigma_l'(\tau) > 0, \qquad \Sigma_u'(\tau) < 0 \tag{93}$$

Solution of (89)–(91) at $T = \tau$, omitting the argument τ for simplicity, gives

$$(S')^2 = \frac{\gamma^2(\Sigma_l' - \Sigma_u')}{\Sigma_l' - \gamma^2\Sigma_u'} \tag{94}$$

which, in view of the signs (93), has a unique positive root which satisfies the required inequality $(81)_1$. $e'(-\tau)$ and $f'(\tau)$ are now given by (90) and (91). The two limit cases in which one $\Sigma_l'(\tau)$ or $\Sigma_u'(\tau)$ is zero also follows from (94), or by direct solution, giving

$$\Sigma_l' \neq 0,\ \Sigma_u' = 0\text{: } S' = \gamma, \qquad e' = f' = 0 \tag{95}$$

$$\Sigma_l' = 0,\ \Sigma_u' \neq 0\text{: } S' = 1, \qquad e' = -\Sigma_u', \qquad f' = 0 \tag{96}$$

in which the initial interface speed is one of the wave speed limits. The smooth change situation in which both $\Sigma_l'(\tau)$ and $\Sigma_u'(\tau)$ are zero is indeterminate from (89)–(91), and requires further differentiation at $T = \tau$.

The final situation is therefore

$$\Sigma_l' = 0,\ \Sigma_u' = 0\text{:} \qquad \Sigma_l'' \leqslant 0,\ \Sigma_u'' \leqslant 0 \tag{97}$$

and it is assumed that one of Σ_l'' or Σ_u'' is non-zero. The second derivatives of (89)–(91) then give

$$e'' + f'' = \Sigma_u'' \tag{98}$$

$$[1 - S']^2 e'' = \frac{1+\gamma}{2\gamma^3}[S' - \gamma]^2\Sigma_l'' \tag{99}$$

$$[1 + S']^2 f'' = -\frac{1-\gamma}{2\gamma^3}[S' - \gamma]^2\Sigma_l'' \tag{100}$$

from which e'' and f'' can be eliminated to yield a quartic equation for S':

$$h(S') = [(1+\gamma)(1+S')^2 - (1-\gamma)(1-S')^2](S'-\gamma)^2\Sigma_l'' - 2\gamma^3[1-(S')^4]\Sigma_u'' = 0. \tag{101}$$

Now

$$h'(S') = 4S'(S'-\gamma)[\gamma(S'-\gamma) + \gamma S' + 3]\Sigma_l'' + 8\gamma^3(S')^3\Sigma_u'' \tag{102}$$

which is strictly negative in $\gamma < S' < 1$, and

$$h(\gamma) = -2\gamma^3(1-\gamma^4)\Sigma_u'' \geqslant 0, \qquad h(1) = 4(1+\gamma)(1-\gamma)^2\Sigma_l'' \leqslant 0 \tag{103}$$

with the equalities if Σ_u'' vanishes, giving $S' = \gamma$, or Σ_l'' vanishes, giving $S' = 1$, respectively, and otherwise a unique root S' of (101) in the open interval. The corresponding e'' and f'' are then given by (99) and (100).

Limit cases in which the stress is applied discontinuously to approximate very rapid change of stress, are also treated. Consider first the case when the entire loading stress is applied as discontinuity at $T = 0$, described by

$$\Sigma_l(\mathrm{T}) = \Sigma_0 H(T),\ T < 0+; \qquad \Sigma(T) = \Sigma_u(T),\ 0+ < T, \qquad \Sigma_u(0+) = \Sigma_0 \tag{104}$$

where $H(T)$ is the Heaviside unit function. The corresponding wave characteristics pattern is shown in Figure 3. The discontinuous loading front propagates from the surface at $T = 0$ with the loading wave speed γ and carries the entire loading; there is no continuous wave $g(Z - \gamma T)$. The interface between loading and unloading regions therefore has the known prescribed constant speed γ. Eventually the discontinuous front is annulled and there is no outgoing loading wave, but as before reloading may arise at some stage and the stress field must be tested to determine the valid domain. The continuous unloading waves are described by

$$T > 0,\ 0 < Z < \gamma T\colon \Sigma = e(Z-T) + f(Z+T), \qquad V = k[e(Z-T) - f(Z+T)] \tag{105}$$

Now the interface path (speed) is known, but the two continuity conditions of stress and particle velocity at the interface are replaced by a single momentum jump condition

$$Z = \gamma T\colon\ [\sigma_z) = \rho c[v], \qquad [\Sigma] = \frac{c}{kc_u}[V] \tag{106}$$

where particle velocity has been neglected in comparison with the wave speed, and here c is $c_l = \gamma c_u$, for the loading front, and γ and k are defined by (69), (72) and (73). Note that the factor $1/k$ is balanced by a factor k in the wave function expressions (105) for V, and will not appear in

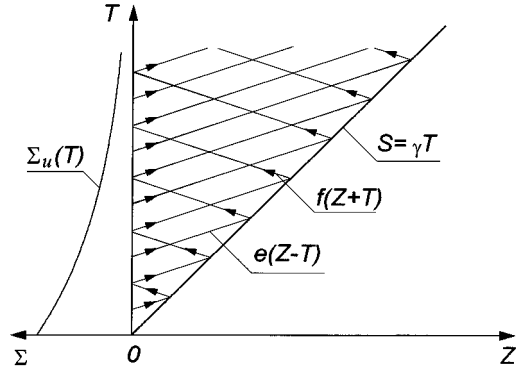

Figure 3. Wave characteristics pattern for a discontinuous load, continuous unload pulse

the resulting wave function relations. The two unknown wave functions $e(Z-\gamma T)$ and $f(Z+\gamma T)$ are determined by an applied continuous surface stress condition $(104)_2$, together with the momentum jump condition $(106)_2$. Thus,

$$T>0:\ e(-T)+f(T)=\Sigma_u(T) \tag{107}$$

and

$$T>0:\ e[-(1-\gamma)T]+f[(1+\gamma)T]=\gamma\{e[-(1-\gamma)T]-f[(1+\gamma)T]\} \tag{108}$$

since the loading front $S=\gamma T$ moves into a region of zero stress and velocity. Eliminating $f[(1+\gamma)T]$ and $e[-(1-\gamma)T]$ in turn gives the algebraic difference equations

$$T>0:\ (1-\gamma)e[-(1-\gamma)T]-(1+\gamma)e[-(1+\gamma)T]=-(1+\gamma)\Sigma_u[(1+\gamma)T] \tag{109}$$

$$T>0:\ (1-\gamma)f[-(1-\gamma)T]-(1+\gamma)f[(1+\gamma)T]=(1-\gamma)\Sigma_u[(1-\gamma)T] \tag{110}$$

for $e[-(1-\gamma)T]$ and $f[(1+\gamma)T]$, with initial values

$$e(0)=\frac{1+\gamma}{2\gamma}\Sigma_u(0),\qquad f(0)=-\frac{1-\gamma}{2\gamma}\Sigma_u(0) \tag{111}$$

The stress, and hence its time derivative, cannot be expressed explicitly in terms of the applied surface stress, so the validity of the assumed unloading domain must be tested for each example.

An alternative case is when the unloading takes place entirely as a discontinuity at $T=1$, described by

$$\Sigma(T)=\Sigma_l(T),\ 0<T<1-;\qquad \Sigma_u(T)=\Sigma_l(1-)[1-H(T-1)],\ 1-<T \tag{112}$$

Figure 4 shows the discontinuous unloading front, which represents the entire outgoing unloading wave, propagating from the surface at $T=1$ with the unloading wave speed. Ahead there is a continuous loading wave $g(Z-\gamma T)$, and it is assumed that continuous unloading continues

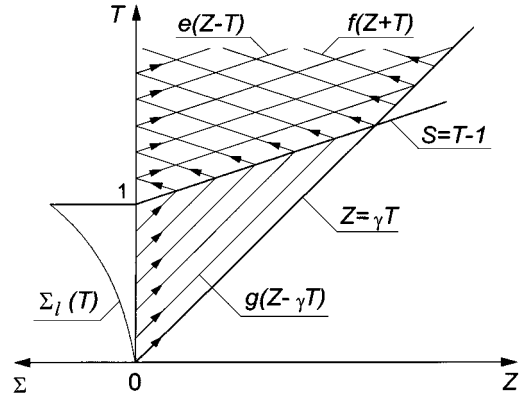

Figure 4. Wave characteristics pattern for a continous load, discontinuous unload pulse

behind the unloading discontinuity front. It is shown that a continuous loading stress such that $\Sigma_1'' > 0$, as depicted, ensures unloading completely back to the surface $Z = 0$, but $\Sigma_1'' < 0$ would require a loading domain to form from the surface at $T = 1$. For convenience let $S(T)$ denote both the path of the unloading discontinuity and the surface $Z = 0$ prior to unloading, so that it is a boundary of the loading domain:

$$0 < T < 1\text{: } S(T) = 0; \qquad T > 1\text{: } S(T) = T - 1 \tag{113}$$

The illustrated wave pattern is defined by

$$T > 0,\ S(T) < Z < \gamma T\text{: } \Sigma = g(Z - \gamma T), \quad V = \frac{k}{\gamma} g(Z - \gamma T) \tag{114}$$

$$T > 1, 0 < Z < T - 1\text{: } \Sigma = e(Z - T) + f(Z + T), \quad V = k[e(Z - T) - f(Z + T) \tag{115}$$

The applied continuous surface stress conditions give

$$0 < T < 1 - \text{: } g(-\gamma T) = \Sigma_1(T); \quad 1 + \ < T\text{: } e(T) + f(T) = 0 \tag{116}$$

which determine $g(-\gamma T)$ explicitly, and relate $e(-T)$ and $f(T)$. Momentum jump across the front gives, for $T > 1+$,

$$e(-1) + f(2T - 1) - \Sigma_1\left[\frac{1 - (1 - \gamma)T}{\gamma}\right] = e(-1) - f(2T - 1) - \frac{1}{\gamma}\Sigma_1\left[\frac{1 - (1 - \gamma)T}{\gamma}\right] \tag{117}$$

Now from $(116)_2$ and (117),

$$e(1 - 2T) = \frac{1 - \gamma}{2\gamma}\Sigma_1\left[\frac{1 - (1 - \gamma)T}{\gamma}\right], f(2T - 1) = -\frac{1 - \gamma}{2\gamma}\Sigma_1\left[\frac{1 - (1 - \gamma)T}{\gamma}\right] \tag{118}$$

and hence

$$\Sigma = \frac{1 - \gamma}{2\gamma}\left\{\Sigma_1\left[\frac{1 + \gamma - (1 - \gamma)(T - Z)}{2\gamma}\right] - \Sigma_1\left[\frac{1 + \gamma - (1 - \gamma)(T + Z)}{2\gamma}\right]\right\} \tag{119}$$

which is an explicit solution for Σ.

Defining the arguments

$$\eta_1 = \frac{1 + \gamma - (1 - \gamma)(T - Z)}{2\gamma}, \qquad \eta_2 = \frac{1 + \gamma - (1 - \gamma)(T + Z)}{2\gamma} \tag{120}$$

the stress variation with time is given by

$$\frac{\partial \Sigma}{\partial T} = \frac{(1 - \gamma)^2}{4\gamma^2}\{-\Sigma_1'[\eta_1] + \Sigma_1'[\eta_2]\} \tag{121}$$

which is negative (confirming unloading) if $\Sigma_1'(\eta_1) > \Sigma_1'(\eta_2)$. Now $\eta_1 > \eta_2$, so unloading is confirmed if $\Sigma_1'' > 0$. Since $\Sigma_1' > 0$, the Σ_1' in term in (121) with argument η_2 depending on $Z + T$, corresponding to the $f(Z + T)$ wave propagated back towards the surface, makes a positive

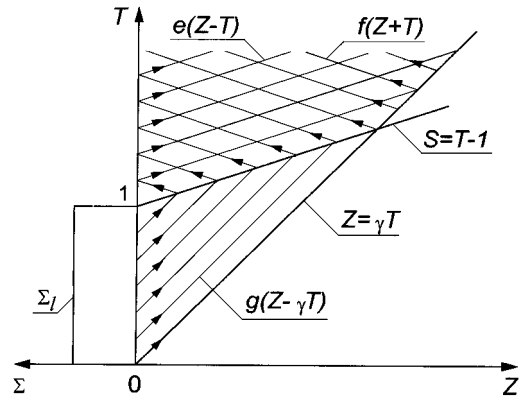

Figure 5. Wave characteristics pattern for a rectangular pulse

contribution to the stress variation with time, while the Σ_1' term with argument η_1 depending on $T - Z$, corresponding to the continuing forward $e(Z - T)$ wave, makes a negative contribution. At a fixed Z, the e wave is initiated from a point on the unloading front nearer the surface, while the f wave is initiated from a point further from the surface, which correspond respectively to intersections at the front of g waves which emerged from the surface at decreasing times. A dominant e wave contribution is associated with increasing stress increments in the applied loading Σ_1. If $\Sigma_1'' < 0$, then the reloading will occur immediately behind the front next to the surface, and a continuous unloading–reloading interface propagates from the surface at $T = 1$, and there is an additional loading region adjacent to the surface. The case $\Sigma_1'' \equiv 0$, corresponding to a linear applied loading stress, is neutral, and the above solution is valid for the entire domain with Σ behind the unloading front linear in Z and independent of T.

A final case considered is a rectangular applied stress which is raised discontinuously to $\Sigma_1(1+)$ at $T = 0$, maintained constant until $T = 1$, then decreased discontinuously back to zero and kept at zero, illustrated in Figure 5. An undisturbed region is entered by the discontinuity loading front with path $Z = \gamma T$, followed by a continuous loading region with outgoing wave $g(Z - \gamma T)$, then the unloading discontinuity front with path $Z = T - 1$, and finally a continuous unloading region with waves $e(Z - T)$ and $f(Z + T)$, and this pattern prevails until the unloading front overtakes the loading front at $T = 1(1 - \gamma)$. Applied stress conditions on $Z = 0$, and momentum jump conditions across the two fronts, show that

$$0 < T < \frac{1}{1-\gamma}, \quad \max(0, T-1) < Z < \gamma T: \Sigma \equiv \Sigma_{1+}, \; V \equiv \frac{k}{\gamma}\Sigma_{1+}, \tag{122}$$

$$T > 1, \; 0 < Z < T - 1: \Sigma \equiv 0, \; V \equiv \frac{k(1-\gamma)}{\gamma}\Sigma_{1+} \tag{123}$$

5. ILLUSTRATIONS

The examples focus on the undrained response with the parameter γ defined by $(70)_2$ and k by $(73)_2$, and the pore pressure P^{f*} generation is governed by (76). Some comparisons are made with

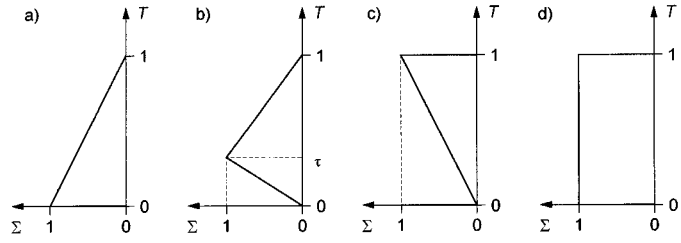

Figure 6. Examples of applies surface pulse

the corresponding free draining response with parameters defined by $(70)_1$ and $(73)_1$, for which the wave speed ratio γ is much smaller, and the physical length scale z^* is a very much smaller. Changes over a unit Z length, therefore, correspond to changes over much shorter physical lengths in free draining response. The compaction evolution is governed by (75) in terms of the dimensionless strain E for both free and undrained response, but differs in terms of stress Σ variation since there are different stress–strain slopes (72) corresponding to the different k and γ.

Figure 6 shows the applied surface stress distributions treated to explore the influence of the loading time τ relative to the unit load–unload time, with discontinuous loading and unloading as limit cases. Values $\tau = 0{\cdot}25, 0{\cdot}5, 0{\cdot}75$ were used. The continuous stress changes are assumed to be linear for simplicity since curvature will not have a significant effect on attenuation or pore pressure. In this case there are explicit algebraic solutions for the constant velocity interface path and linear wave functions in all cases, which were used as test cases for the numerical algorithm constructed to solve the general non-linear relations. The compaction evolution equation (75) is always non-linear. Illustrations are now presented for the limit cases $\tau = 0$, $\tau = 1$ and the rectangular pulse, and for the continuous pulse with rise time $\tau = 0{\cdot}5$. Figures 7 and 8 compare the compaction profiles at different times in free draining and undrained conditions for the case $\tau = 0$. There is a significant difference in the profile shapes between free draining and undrained conditions, but also in the compaction amplitudes with that in undrained conditions a factor 0·05 of that in free draining, due to the buoyancy or resisting effect of the pore pressure. The corresponding axial stress and pore pressure profiles are shown in Figure 9, with distinct differences in the axial stress profiles for free draining and undrained conditions, both in the pulse shape evolution and the length and time scales of decay. The residual pore pressure in undrained conditions is small compared to the original pulse amplitude, but unlike the propagating axial stress pulse, does not decrease with time. Figures 10 and 11 illustrate the axial stress and pore pressure profiles for undrained conditions for the case $\tau = 1$ and the rectangular pulse, showing again the amplitude and pulse length decay. Finally, Figure 12 shows the axial stress and pore pressure for undrained conditions, and axial stress for free draining, for the continuous pulse with $\tau = 0{\cdot}5$, with contrasting pulse shape evolutions and length and time scales of decay.

A general note is that the effects of wave interactions across the load–unload interface are significant for free draining where the loading and unloading wave speeds are very different, and here the actual non-linearity of the stress–strain paths and consequent non-uniform wave speeds would also be significant. However, for undrained conditions the constant wave speeds approximation is much better, and further, the small difference between loading and unloading wave

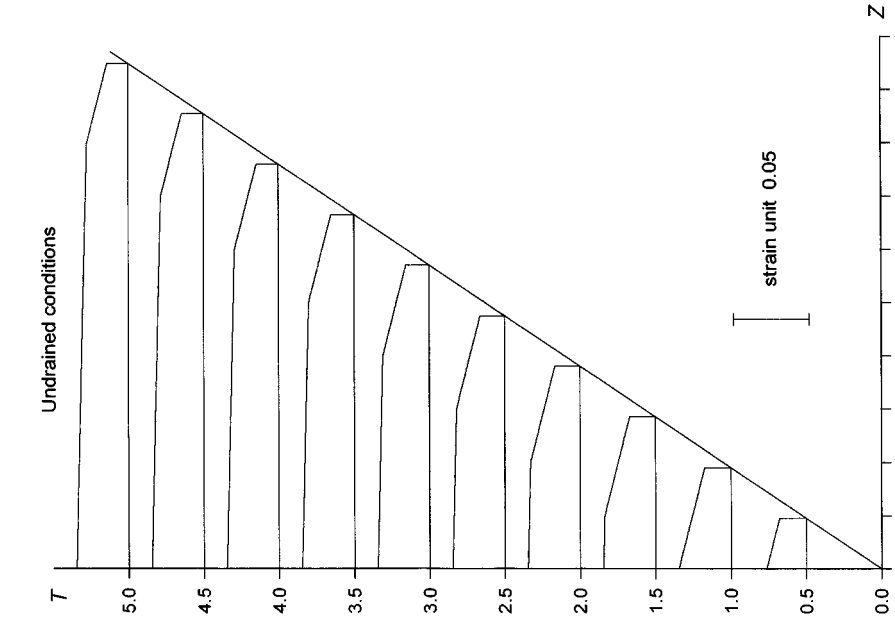

Figure 8. Compaction profiles in undraining conditions for $\tau = 0$

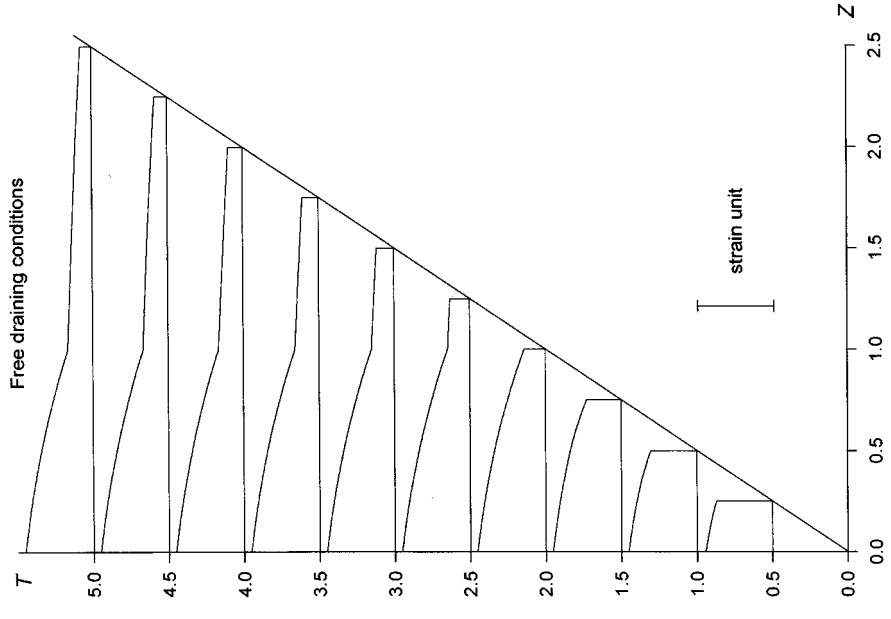

Figure 7. Compaction profiles in free draining conditions for $\tau = 0$

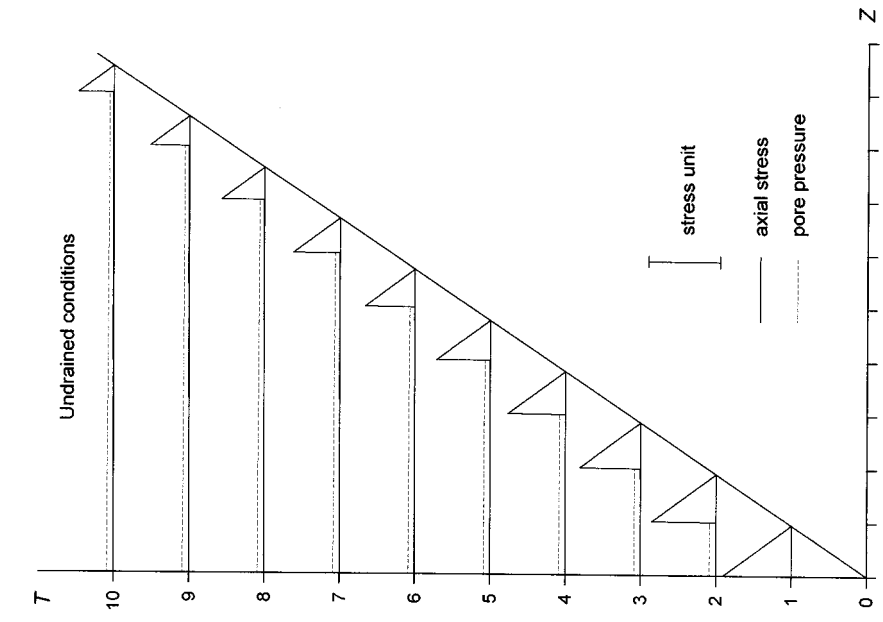

Figure 10. Axial stress and pore pressure (– – –) profile in undrained conditions for $\tau = 1$

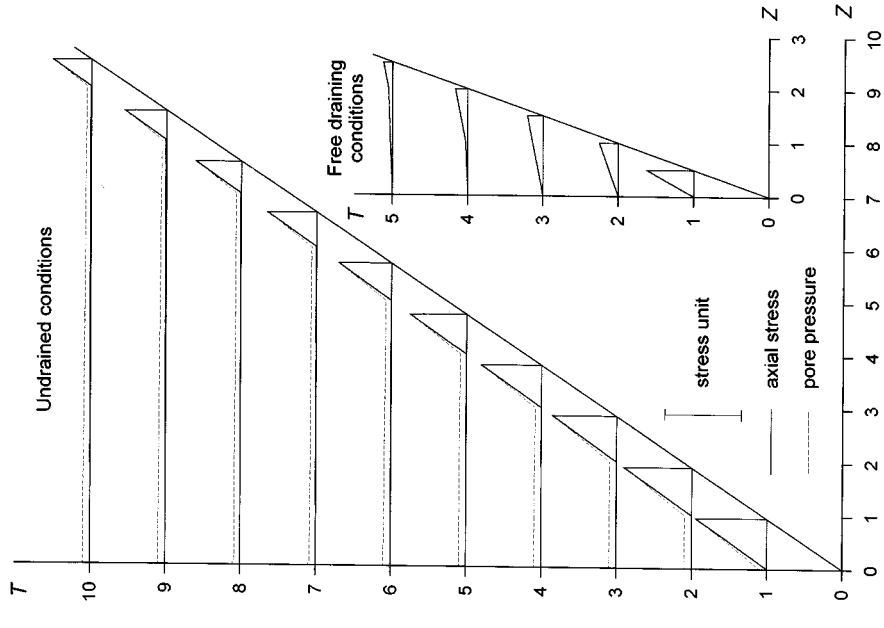

Figure 9. Axial stress and pore pressure (– – –) profiles in free draining and undrained conditions for $\tau = 0$

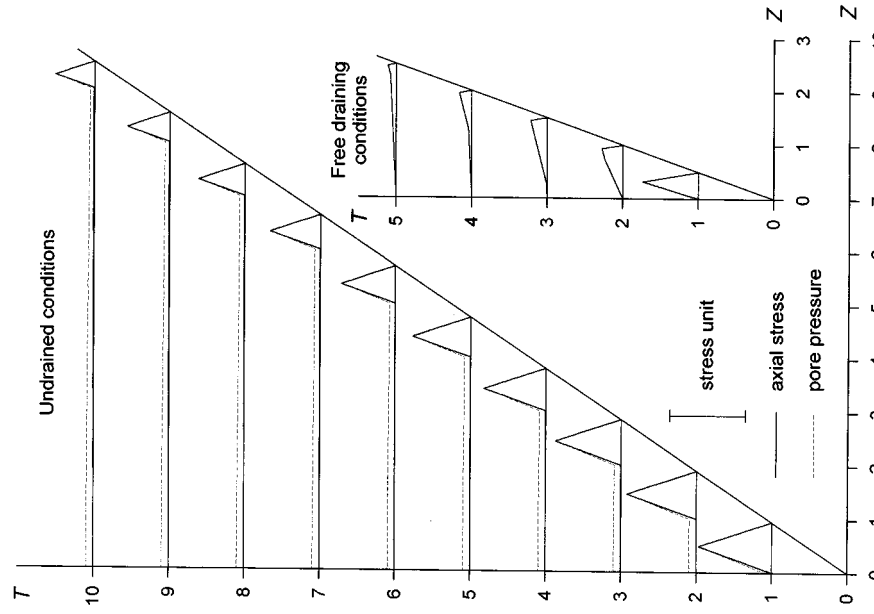

Figure 12. Axial stress and pore pressure (– – –) profiles in free draining and undrained conditions for $\tau = 0{\cdot}5$

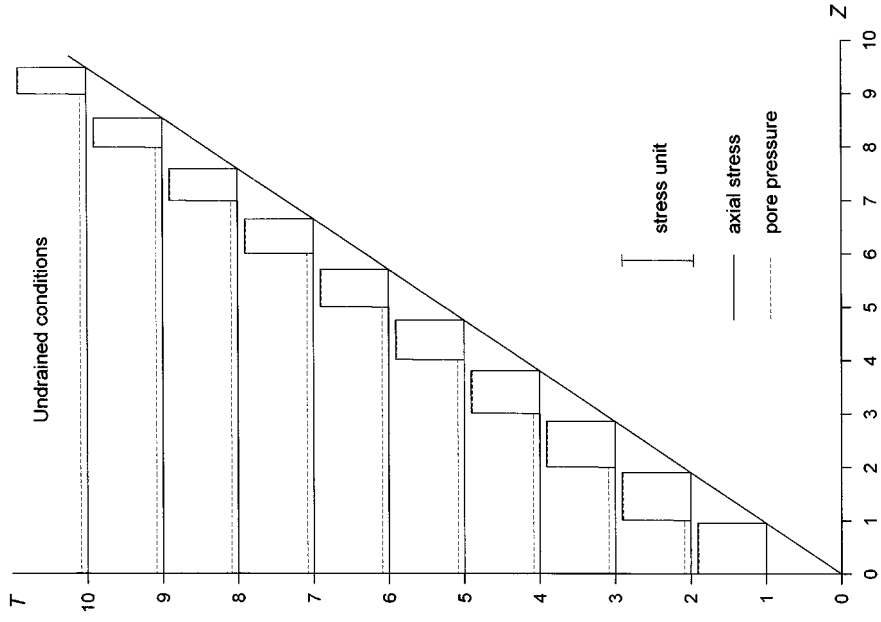

Figure 11. Axial stress and pore pressure (– – –) profiles in undrained conditions for a rectangular pulse

speeds render the wave interactions less significant so that a simpler common stress–strain path and wave speed theory may be adequate.

REFERENCES

1. O. C. Zienkiewicz, 'Generalised plasticity and some models for geomechanics', *Appl. Math. Mech.*, **3,** 303–318 (1982).
2. K. C. Valanis, 'A theory of viscoplasticity without a yield surface. Part I. General theory', *Arch. Mech.*, **23,** 517–533 (1971).
3. Z. P. Bažant and R. J. Krizek, 'Saturated sand as an inelastic two-phase medium', *Proc. ASCE, J. Engng. Mech. Div.*, **101,** 317–332 (1975).
4. Z. P. Bažant and R. J. Krizek, 'Endochronic constitutive law for liquefaction of sand', *Proc. ASCE, J. Engng. Mech. Div.*, **102,** 225–238 (1976).
5. L. W. Morland, 'A simple constitutive theory for a fluid-saturated porous solid', *J. Geophys. Res.*, **77,** 890–900 (1972).
6. L. W. Morland, 'A theory of slow fluid flow through a porous thermoelastic matrix', *Geophys. J. Roy. Astronom. Soc.*, **55,** 393–410 (1978).
7. L. W. Morland and A. Sawicki, 'A mixture model for the compaction of saturated sand', *Mech. Mater.* **2,** 203–216 (1983).
8. L. W. Morland and A. Sawicki, 'A model for compaction and shear hysteresis in saturated granular materials', *J. Mech. Phys. Solids*, **33,** 1–24 (1985).
9. A. Sawicki and L. W. Morland, 'Dynamic shear response of a granular column', S. K. Saxena (ed.) *Proc. US Engng. Found. Conf. Compressibility Phenomena in Subsidence*, 1986, pp. 3–30.
10. A. Sawicki and L. W. Morland, 'Pore pressure generation in a saturated sand layer subjected to a cyclic horizontal acceleration at its base', *J. Mech. Phys. Solids*, **33,** 545–559 (1985).
11. L. W. Morland, 'Compaction and shear settlement of granular materials', *J. Mech. Phys. Solids*, **41,** 507–530 (1993).
12. L. W. Morland, A. Sawicki and P. C. Milne, 'Uni-axial compaction of the granular material', *J. Mech. Phys. Solids*, **41,** 1755–1779 (1993).
13. L. W. Morland, 'Flow of viscous fluids through a porous deformable matrix', *Surveys Geophys.*, **13,** 209–268 (1992).
14. M. Mokni, 'Relations entre deformations en masse et deformations localisees dans les materiaux granulaires', Ph.D. Thesis, Institut de Mecanique de Grenoble, France, 1992.
15. B. A., Schrefler, L. Sanavia and C. E. Majorana, 'A multiphase medium model for localisation and postlocalisation simulation in geomaterials', *Mech. Cohesive–Frictional Mater.* **1,** 95–114 (1996).
16. L. W. Morland, 'The propagation of plane irrotational waves through an elastoplastic medium', *Phil. Trans. Roy. Soc.*, **A251,** 341–383 (1959).
17. L. M. Morland and A. D. Cox, 'Existence and uniqueness of solutions to uni-axial elastic-plastic wave interactions', *Phil. Trans. Roy. Soc.*, **A264,** 479–556 (1969).
18. A. Sawicki and W. Swidzinski, 'Mechanics of a sandy subsoil subjected to cyclic loadings', *Int. J. Numer. Anal. Methods Geomech.*, **13,** 511–529 (1989).

